

A QBO cookbook: Sensitivity of the Quasi-Biennial Oscillation to resolution, resolved waves, and parameterized gravity waves

Chaim I. Garfinkel¹, Edwin P. Gerber², Ofer Shamir¹, Jian Rao^{1,4}, Martin
Jucker³, Ian White¹, Nathan Paldor¹

¹Fredy and Nadine Herrmann Institute of Earth Sciences, Hebrew University, Jerusalem, Israel.

²Courant Institute of Mathematical Sciences, New York University, New York, USA

³Climate Change Research Centre and ARC Centre of Excellence for Climate Extremes, University of
New South Wales, Sydney, Australia

⁴ Key Laboratory of Meteorological Disaster, Ministry of Education (KLME) / Joint International
Research Laboratory of Climate and Environment Change (ILCEC) / Collaborative Innovation Center on
Forecast and Evaluation of Meteorological Disasters (CIC-FEMD), Nanjing University of Information
Science and Technology, Nanjing 210044, China

Key Points:

- Sensitivity of the QBO to resolution, dissipation, wave forcing, and parameterized gravity waves is explored in a single framework.
- The QBO period can be tuned independently of its amplitude, but the vertical structure (particularly at lower levels) is harder to capture.
- The influence of factors on the QBO can be related to their impact on wave-induced momentum fluxes in the deep tropics.

Corresponding author: Chaim I. Garfinkel, chaim.garfinkel@mail.huji.ac.il

21 **Abstract**

22 An intermediate complexity moist General Circulation Model is used to investigate the
 23 sensitivity of the Quasi-Biennial Oscillation (QBO) to resolution, diffusion, tropical tro-
 24 pospheric waves, and parameterized gravity waves. Finer horizontal resolution is shown
 25 to lead to a shorter period, while finer vertical resolution is shown to lead to a slower
 26 period and to an accelerated amplitude in the lowermost stratosphere. More scale-selective
 27 diffusion leads to a faster and stronger QBO, while enhancing the sources of tropospheric
 28 stationary wave activity leads to a weaker QBO. In terms of parameterized gravity waves,
 29 broadening the spectral width of the source function leads to a longer period and a stronger
 30 amplitude although the amplitude effect saturates when the half-width exceeds $\sim 25\text{m/s}$.
 31 A stronger gravity wave source stress leads to a faster and stronger QBO, and a higher
 32 gravity wave launch level leads to a stronger QBO. All of these sensitivities are shown
 33 to result from their impact on the resultant wave-driven momentum torque in the trop-
 34 ical stratosphere. Atmospheric models have struggled to accurately represent the QBO,
 35 particularly at moderate resolutions ideal for long climate integrations. In particular, cap-
 36 turing the amplitude and penetration of QBO anomalies into the lower stratosphere (which
 37 has been shown to be critical for the tropospheric impacts) has proven a challenge. The
 38 results provide a recipe to generate and/or improve the simulation of the QBO in an at-
 39 mospheric model.

40 **Plain Language Summary**

41 The most prominent mode of variability in the tropical stratosphere is the quasi-
 42 biennial oscillation (QBO), however only relatively recently have comprehensive mod-
 43 els begun to simulate a QBO spontaneously, and even in these models the representa-
 44 tion of the QBO typically suffers from biases. Here we elucidate the sensitivities of the
 45 QBO to a wide range of model parameters, and explore how these parameters affect the
 46 QBO behavior. We expect that these results will be helpful for tuning of more compre-
 47 hensive models.

48 **1 Introduction**

49 The dominant mode of variability in the tropical stratosphere, the Quasi-Biennial
 50 Oscillation, consists of downward propagating easterly and westerly wind regimes, with
 51 a period typically ranging from 24 to 32 months (Baldwin et al., 2001). Although the

52 QBO is a tropical phenomenon, it impacts the atmospheric circulation and composition
 53 globally through a variety of mechanisms. One of the earliest remote influences to be rec-
 54 ognized is the so-called “Holton-Tan effect” whereby the QBO modulates the strength
 55 of the stratospheric polar vortex (Holton & Tan, 1980; Garfinkel et al., 2012; Anstey &
 56 Shepherd, 2014; Rao et al., 2020b), and this effect is projected to intensify under climate
 57 change (Rao et al., 2020c). The QBO also directly influences tropospheric variability by
 58 affecting the Pacific subtropical jet (Garfinkel & Hartmann, 2011a, 2011b) and tropical
 59 convection on both seasonal mean (Collimore et al., 2003; Liess & Geller, 2012; Rao et
 60 al., 2020a) and subseasonal timescales (Yoo & Son, 2016; Zhang & Zhang, 2018; Mar-
 61 tin et al., 2019). QBO signals are also evident in temperature and in stratospheric con-
 62 stituents such as ozone and water vapor (Randel & Wu, 1996; Randel et al., 1998; Di-
 63 allo et al., 2018; Tian et al., 2019).

64 The QBO is driven by waves propagating upwards from the troposphere with pe-
 65 riods unrelated to (and much faster than) that of the resulting oscillation. Lindzen and
 66 Holton (1968) showed how a QBO could be driven by a broad spectrum of vertically prop-
 67 agating waves (with phase speeds in both westward and eastward directions), in which
 68 a two-way feedback between the waves and the background flow leads to oscillating winds.
 69 The first part of the feedback is that the background flow modulates the propagation
 70 and damping/dissipation of the waves. The second part of the feedback is that when the
 71 waves experience damping or dissipation, they flux momentum to the background flow.
 72 Holton and Lindzen (1972) and Plumb (1977) demonstrated that only two wave modes
 73 (one with easterly and one with westerly phase speeds) are required as long as dissip-
 74 ation of waves occurs near, and not solely at, the critical lines. An important implication
 75 of this earlier work is that the period and amplitude of the oscillation are controlled, in
 76 part, by the spectral range and amplitude of the momentum fluxed by these waves. The
 77 particular waves associated with the QBO was the focus of later work, and both large-
 78 scale waves (especially Kelvin waves for the westerly regime) and smaller scale gravity
 79 waves have been found to be crucial (Ern et al., 2014; Pahlavan et al., 2021).

80 While the first models began to successfully simulate a spontaneous QBO-like os-
 81 cillation some 20 years ago (Takahashi, 1996, 1999; Scaife et al., 2000; Hamilton et al.,
 82 2001), only around five models participating in Coupled Model Intercomparison Project
 83 Phase 5 (CMIP5) spontaneously simulated it, and the majority of CMIP6 models still
 84 have no QBO (Richter et al., 2020; Rao et al., 2020a, 2020b). Even in CMIP models that

succeed in simulating a QBO with period and amplitude relatively close to that observed, the QBO winds suffer from an inability to propagate downwards to the lower stratosphere, a bias also evident in models participating in the Quasi-Biennial Oscillation initiative (QBOi; Bushell et al., 2020). Furthermore, the representation of the waves that fundamentally drive the QBO differ dramatically among the QBOi models (Holt et al., 2020), with e.g., Kelvin wave activity barely evident in some models while too strong in others. Diversity in the representation of mixed Rossby-gravity waves, which also contributes to the driving of the QBO, is even more pronounced (Holt et al., 2020). The models with stronger convectively coupled waves rely less heavily on zonal mean forcing from parameterized gravity waves (Holt et al., 2020). All but one of these models (the MIROC model) also includes a parameterization of gravity waves (Bushell et al., 2020), as the resolved waves are apparently not energetic enough to force the QBO at resolutions typically used by these models.

The QBO is sensitive not only to the generation of resolved wave modes, but also to their subsequent upwards propagation. Some of the resolved waves have a characteristic vertical wavelength of a few kilometers (figure 8 and 10 of Kiladis et al., 2009), and hence a model with, say, a vertical resolution of a kilometer (which is typical of CMIP and QBOi models in the lowermost stratosphere, Butchart et al., 2018) will not be able to accurately represent its upward propagation. The net effect is that the resolved wave forcing that reaches the QBO region, and hence the QBO itself, is influenced by vertical resolution (Geller et al., 2016; Anstey et al., 2016). Indeed, Holt et al. (2016) explored a model with 7km horizontal resolution that included a realistic resolved wave spectrum and plentiful small-scale gravity waves in the troposphere, but still required parameterized gravity waves due to a poor representation of resolved wave dissipation in the shear zones, due in part to the relatively coarse vertical resolution. The fact that at least twenty different CMIP and QBOi models still simulate a reasonable QBO reflects the fact that these models tune the parameterized gravity waves so that the overall momentum forcing is sufficient.

The goal of this study is to identify and isolate the role of resolution, dissipation, resolved wave forcing, and parameterized wave forcing, for the QBO. While many of these sensitivities have been reported before, here we assess a broader range of sensitivities all within a single modeling framework. While it is possible to consider these factors in a multi-model ensemble such as QBOi or CMIP6, the wide diversity in the representation

of these factors among the models limits the confidence with which one can ascribe changes to a given cause. For example, the tropical climatology in comprehensive GCMs is (with good reason) made as realistic as possible, which necessarily limits the ability to examine how changing resolved waves impacts the QBO. It is also very difficult to perturb the resolution of a comprehensive model without severely altering its climatology, given the need to re-tune other scale-sensitive parameterizations. Here, we explore the role of these three factors for the QBO in a single modeling framework, with the expectation that results in our framework may be relevant to other models. Our hope is that these results can be used to more intelligently tune other models.

After describing the model and the gravity wave scheme in Section 2, we document the sensitivity to resolution, the gravity wave scheme, the hyperdiffusion, and the resolved waves in Section 3. We then explain how these various perturbations to the model lead to changes in QBO periodicity and downward propagation to the lower stratosphere in Section 4. We summarize our results and conclude with an example use of the cookbook to improve the QBO of our control integration in Section 5.

2 A Model of an idealized Moist Atmosphere (MiMA)

We use the model of an idealized moist atmosphere (MiMA) introduced by Jucker and Gerber (2017), Garfinkel et al. (2020a), and Garfinkel et al. (2020b). This model builds on the aquaplanet models of Frierson et al. (2006), Frierson et al. (2007), and Merlis et al. (2013). Very briefly, the model solves the moist primitive equations on the sphere, employing a simplified Betts-Miller convection scheme (A. K. Betts, 1986; A. Betts & Miller, 1986), idealized boundary layer scheme based on Monin-Obukhov similarity theory, a slab ocean, and the Rapid Radiative Transfer Model (RRTMG) radiation scheme (Mlawer et al., 1997; Iacono et al., 2000). Please see Jucker and Gerber (2017) and Garfinkel et al. (2020b) for more details. Orography, ocean zonal heat transport, and land-sea contrast (i.e., difference in heat capacity, surface friction, and moisture availability between oceans and continents) are specified as in Garfinkel et al. (2020b).

The details of the gravity wave scheme (developed by Alexander & Dunkerton, 1999) are included in the appendix. Unless otherwise indicated, all simulations in this paper were run with a triangular truncation at wavenumber 42 (T42; equivalent to a roughly

148 2.8° grid) with 40 vertical levels and a model top at 0.18hPa, for 38 years after discarding
 149 at least 10 years as spinup.

150 This specification allows for a reasonable mean state in the model. Figure 1a shows
 151 the December through February climatology of the zonal winds in a control simulation
 152 (hereafter CONTROL) at T85 resolution, and Figure 1b shows the standard deviation
 153 of the winds. The model simulates a reasonable stratospheric and tropospheric mean state,
 154 and robust variability in the tropical stratosphere. The mean state in the tropical strato-
 155 sphere suffers from a westerly bias, however, and this leads to the QBO in our model suf-
 156 fering from a too-strong westerly regime, and concomitantly, too-weak an easterly regime.
 157 Gupta et al. (2020) found that such a bias occurs more commonly in spectral cores, as
 158 compared to, say, finite volume. Such a bias is also evident in some of the QBOi mod-
 159 els examined by Bushell et al. (2020, see their figure 2) and CMIP6 models examined
 160 by Rao et al. (2020b, see their figure 1). Future work should confirm whether the sen-
 161 sitivities found here are robust in a model which does not suffer from this bias. Finally,
 162 midlatitude stationary waves, tropical precipitation, and stratospheric variability in CON-
 163 TROL were found to be captured as well as many CMIP models (Garfinkel et al., 2020a,
 164 2020b; White et al., 2020). As shown later, the model represents tropical wave modes
 165 realistically as well.

166 We focus on the sensitivity of these key metrics of the QBO: the vertical structure
 167 of its amplitude, quantified by the standard deviation of zonal mean zonal winds at 20hPa
 168 and at 77hPa representing the mid- and lower-stratosphere respectively¹, and the pe-
 169 riodicity, quantified by the peak power of the Fourier transformed zonal mean zonal wind
 170 at 27hPa. We focus on the period at 27hPa as the QBO is well-defined at this level even
 171 in simulations with a weak QBO. All of these metrics are computed after first applying
 172 a low-pass ninth-order Butterworth filter with a cutoff at 120 days in order to remove
 173 high frequency wave-driven variability. The simulations performed, and the value of these
 174 metrics for each simulation, are listed in Figure 2. Note that the correlation between the
 175 amplitude at 27hPa and the period across all simulations is small (0.11), while the cor-
 176 relation between the amplitude at 20hPa and 77hPa is 0.81. This immediately suggests

¹ Such a definition can be used even in cases with a poorly defined QBO, unlike definitions which ex-
 plicitly quantify wind maxima.

177 greater flexibility in tuning the period independently of the overall amplitude than in
 178 tuning the vertical structure of the QBO.

179 **3 Survey of sensitivity to resolution, dissipation, resolved waves, and**
 180 **gravity waves**

181 We first consider the sensitivity of the QBO to resolved processes, keeping the set-
 182 tings for the gravity wave scheme fixed, in Section 3.1. Section 3.2 then presents the sen-
 183 sitivity to the gravity wave scheme while keeping the numerics and boundary conditions
 184 fixed.

185 **3.1 Sensitivity to resolution, dissipation, and tropospheric stationary**
 186 **waves**

187 Figure 3a shows the QBO in the ERA5 reanalysis (Hersbach et al., 2020; Pahla-
 188 van et al., 2021, the QBO is similar in other reanalyses) and Figure 3b shows the QBO
 189 at T42 with 40 vertical levels in our CONTROL. At this resolution, MiMA simulates a
 190 QBO similar to that observed: the period is slightly longer, but as shown later, relatively
 191 small changes to the settings in the model can lead to an exact match. The standard de-
 192 viation of winds in the mid-stratosphere is realistic, though it is under-estimated lower
 193 in the stratosphere. Too-weak QBO winds in the lower stratosphere is a common bias
 194 in QBOi and CMIP6 models (Richter et al., 2020; Rao et al., 2020a; Bushell et al., 2020),
 195 and the factors that lead to its amelioration will be discussed shortly.

196 If the number of vertical levels is increased by a factor of 3, with the extra levels
 197 added in-between the existing levels while the model lid is kept fixed, the QBO period
 198 lengthens to 4.1 years (consistent with the lengthening of the period found in the model
 199 of Anstey et al., 2016), while the standard deviation in the lowermost stratosphere in-
 200 creases by more than $\sim 50\%$ (Figure 3c; similar to the effect in the model of Geller et
 201 al., 2016). A *decrease* in the number of vertical levels has an opposite effect (Figure 3d):
 202 a shorter period and a degradation in the standard deviation in the lowermost strato-
 203 sphere, though the standard deviation in the mid-stratosphere is unaffected. These changes
 204 are summarized in Figure 4ab, which shows that both the standard deviation in the low-
 205 ermost stratosphere and the period increase monotonically as vertical resolution is in-
 206 creased. If the horizontal resolution is increased to T63 or T85 (Figure 3ef, roughly equiv-
 207 alent to a grid of 1.9° or 1.4°), the period decreases to 1.75 years and 1.2 years respec-

tively. The amplitude increases for the T63 integration (consistent with Giorgetta et al. (2006)), but then decreases as the resolution is further increased to T85 (Giorgetta et al., 2006, did not consider T85 and we are not aware of any other relevant study). These changes are summarized in Figure 4cd: the period decreases monotonically as horizontal resolution is increased, while the amplitude changes are less clear.

Models also differ in how they specify horizontal diffusion (Table 7 of Butchart et al., 2018), and early modeling studies found sensitivity to this parameter (Takahashi, 1996). In our pseudo-spectral model, the order n of the hyperdiffusion operator $\kappa \nabla^n$ governs the extent to which the diffusion is scale-selective. Larger n leads to greater scale-selectivity, and a smaller impact of diffusion on the large scale features. The net effect is that wavenumbers above the smallest resolved scale (i.e., 40 or 41 for T42) are damped more strongly if the damping order n is, say, 6 (i.e., ∇^6 hyperdiffusion) than if $n = 10$. The CONTROL hyperdiffusion is ∇^8 , and we explore sensitivity to $n = 6$ and $n = 10$ in Figure 4ef; in all cases, we modify the hyperdiffusion coefficient κ such that the damping of the highest resolved wavenumber (42 at T42) is fixed so as to not impact the numerical stability of the model. Lowering n to 6 or raising it to 10 has a strong impact on the QBO amplitude: a lower value of n leads to a weaker QBO with an essentially unchanged period (Supplemental Figure 1a and Figure 4ef), while a larger value of n leads to a stronger QBO with a shorter period (Supplemental Figure 1b). This effect is due to the weaker damping on small scale resolved waves for a larger value of n .

Next, we explore sensitivity of the QBO to tropospheric stationary waves, while keeping other settings fixed. The stationary waves in CONTROL compare favorably to those observed (Garfinkel et al., 2020a, 2020b), and as shown in Shamir et al. (2021) and Section 4.1, resolved tropical transient waves are reasonable as well. In order to quantify the impact of tropospheric stationary waves on the QBO, we remove land-sea contrast, orography, and east-west oceanic heat transport (as discussed in detail in Garfinkel et al. (2020a) and Garfinkel et al. (2020b)), while keeping the north-south oceanic heat transport of Jucker and Gerber (2017). The resulting weakening of the stationary waves leads to a strengthening of the QBO by over 50% in both the mid-stratosphere and lower-stratosphere (zonally symmetric BC run in Figure 2 and Supplemental Figure 1c) and also to a slight decrease in the period.

239 Overall, the properties of the QBO are sensitive to the treatment of resolved waves
 240 while holding the gravity wave drag fixed. Specifically, the resolution, horizontal diffu-
 241 sion, and stationary waves all impact the QBO.

242 **3.2 Sensitivity to gravity waves**

243 We now turn our attention to the sensitivity of the QBO to the settings of the grav-
 244 ity wave scheme, taking CONTROL with T42 and 40 levels as the starting point. One
 245 of the tunable parameters in the Alexander and Dunkerton (1999) GW scheme (and in-
 246 deed of any GW scheme) is the spectral width of the forced gravity waves (c_w in equa-
 247 tion A1). If c_w is decreased, then the gravity waves launched in the scheme will have a
 248 narrower range of phase speeds. The idealized models of Holton and Lindzen (1972) and
 249 Plumb (1977) predict that such a narrowing of launched phase speeds will lead to a de-
 250 crease in the amplitude of the QBO winds. We now test this prediction here. In CON-
 251 TROL, $c_w = 35\text{m/s}$, and we explore sensitivity to changing this parameter in Figure
 252 4gh and Supplemental Figure 2. Note that c_w is only changed from 10S to 10N (i.e. $c_w =$
 253 35m/s outside of the tropics) so as to not directly impact the representation of the mid-
 254 latitude and polar stratosphere and minimally impact polar downwelling. The QBO is
 255 increasingly sensitive to c_w if c_w is less than around 25m/s . For $c_w = 5\text{m/s}$, the QBO
 256 essentially disappears, and for a $c_w = 15\text{m/s}$ the QBO standard deviation is little more
 257 than half of the standard deviation in the CONTROL integration and the period decreases.
 258 For c_w of 25m/s or higher, however, the resulting QBO is little changed, and it appears
 259 there is a saturation effect in the period and to a lesser degree in the amplitude in the
 260 mid-stratosphere, even as the lower stratospheric amplitude continues to increase (Fig-
 261 ure 4gh).

262 An additional parameter of the gravity wave scheme in our model is B_{eq} , the to-
 263 tal amplitude of the launched gravity wave stress in the tropics (see equation A3); again,
 264 this is a common parameter of most GW schemes. In CONTROL, B_{eq} is set to be iden-
 265 tical to the global value B_0 (which is 0.0043Pa), but this parameter is poorly constrained
 266 by observations and models often use higher or lower values (Figure 5 of Molod et al.,
 267 2012). Figure 4ij and Supplemental Figure 3 assess sensitivity to the value of this pa-
 268 rameter. Lowering B_{eq} leads to a weakening of the QBO, as might be expected, with a
 269 slight decrease in the period. Increasing B_{eq} leads to a stronger QBO and to a sharper
 270 decrease in the period. That a stronger B_{eq} leads to a shorter period is consistent with

271 Figure 1 of Geller et al. (2016), Table 2 of Rind et al. (2014), Figure 13 of Giorgetta et
 272 al. (2006), and section 3.4 of Richter et al. (2014). We find, however, that the sensitiv-
 273 ity of the period is non-monotonic (Figure 4ij).

274 A final parameter of the gravity wave scheme which is poorly constrained is the
 275 vertical level at which gravity waves are launched. The launch height in our setup is the
 276 sigma ($\frac{p}{p_s}$, where p_s is the surface pressure) level closest to, but smaller than, 0.315, but
 277 other models launch at 100hPa or even higher up (Anstey et al., 2016). Raising the launch
 278 level leads to a stronger QBO, and as an example we show in Supplemental Figure 3e
 279 the QBO for a launch height of sigma=0.15 and c_w in the tropics of 25m/s (as in Sup-
 280 plemental Figure 2c). The QBO in Supplemental Figure 3e has a larger standard devi-
 281 ation than in Supplemental Figure 2c (which has a launch height at sigma=0.315) in both
 282 the mid- and lower- stratosphere as fewer gravity waves are filtered out before entering
 283 the stratosphere (Figure 2).

284 The sensitivities of the QBO to all of these model properties are summarized in Ta-
 285 ble 1. A wide range of “tuning knobs” are available, and while in our experiments the
 286 T42L40 QBO is closest to that observed outside of the lowermost stratosphere, this was
 287 the product of extensive tuning. A higher resolution version of the model could be tuned
 288 to also reproduce the QBO period and amplitude as well, a point we return to in the dis-
 289 cussion.

290 4 Making sense of the changes in period and downward propagation 291 to the lowermost stratosphere

292 Section 3 demonstrated that the QBO periodicity and downward propagation to
 293 the lower stratosphere are sensitive to a wide range of model parameters. We now seek
 294 to diagnose why. We focus on the metrics included in Figure 2, specifically the period-
 295 icity and the standard deviation at 77hPa (i.e., in the lower stratosphere). This section
 296 considers not only the simulations discussed in Section 3 listed in Figure 2, but also sim-
 297 ulations included in Garfinkel et al. (2020a) and Garfinkel et al. (2020b). As these facets
 298 of the QBO are intimately connected to the location of (pseudo-)momentum fluxes as-
 299 sociated with resolved and parameterized waves, we first consider the generation of re-
 300 solved waves.

301 **4.1 Generation of resolved waves**

302 The QBO is driven in part by transient waves well resolved at T42, and hence we
 303 show in Figure 5 the resolved waves in CONTROL and in ERA-5 reanalysis for zonal
 304 wind at 200hPa from 15S to 15N. MiMA captures the redness of the spectrum in both
 305 time and wavenumber (Garfinkel et al., 2021; Shamir et al., 2021). It also exhibits en-
 306 hanced power near the analytically predicted dry wave modes of Matsuno (1966), as is
 307 evident for Kelvin waves in the symmetric spectrum near a phase speed of 25 m/s. The
 308 spectrum is qualitatively similar in all resolutions in MiMA. There are differences be-
 309 tween the observed spectrum and the spectrum in MiMA, however, and we focus on these
 310 differences in Supplemental Figure 4. At all resolutions, the power is too strong except
 311 for symmetric $\omega - k$ combinations near the Madden Julian Oscillation ($k < 10$ and low
 312 frequencies) which MiMA lacks. Note that Figure 5 and Supplemental Figure 4 show the
 313 logarithm base-10 of the power. Hence a difference of 0.5 in Supplemental Figure 4 means
 314 $\log_{10}(\text{MiMA}) - \log_{10}(\text{ERA5}) = 0.5$, or that MiMA has a factor of $10^{-5} \sim 3x$ more power.
 315 The bias in MiMA approaches a factor of three for $\omega - k$ combinations that are most
 316 energetic in Figure 5, however such a bias is well within the range of biases in the QBOi
 317 models evaluated by Holt et al. (2020).

318 The spectrum closer to the base of the QBO is of more relevance for wave driving
 319 of the QBO. Hence we show the resolved wave spectrum at 77hPa in Figure 6. It is ev-
 320 ident that the simulations with 40 vertical levels struggle to simulate the mixed Rossby-
 321 gravity mode (and to a lesser degree the Kelvin mode), while the simulation with 120
 322 levels does capture these waves (Figure 6f vs 6h for Kelvin, and Figure 6e vs 6g for the
 323 mixed mode). Hence, while resolved waves in the troposphere are similar for different
 324 vertical resolutions, resolved waves higher up differ more strongly. The implications for
 325 the QBO periodicity and downward propagation will be considered in section 4.2 and
 326 4.3.

327 **4.2 Explaining the QBO period**

328 We now attempt to quantify how resolved and parameterized waves drive the dif-
 329 ferences in the period of the QBO among these simulations. In order to do so, we first
 330 consider how the QBO is driven by these waves in CONTROL and then consider how
 331 this wave-driving differs among the other experiments.

332 Taking CONTROL at T85 as an example, the top row of Figure 7 shows the zonal
 333 wind tendency due to parameterized gravity waves and resolved waves (i.e., the Eliassen-
 334 Palm flux divergence or EPFD) for a westerly QBO phase in the lower stratosphere (anal-
 335 ogous to Figure 8 of Manzini et al. (2006) and Figure 13 of Holt et al. (2020)), defined
 336 as winds at 40hPa between 10m/s and 15m/s stronger than climatological. The anomalous
 337 QBO winds are shown in solid brown and dashed blue. Similar to these previous
 338 modeling studies, gravity wave and EPFD from resolved waves are of similar importance
 339 in the lower stratosphere. Higher up, gravity waves dominate the forcing. The wave forc-
 340 ing is concentrated in the shear zones, and hence acts to propagate the anomalous QBO
 341 winds downward. The forcing is quantitatively similar but of opposite sign for the QBO
 342 phase with easterly winds in the lower stratosphere (bottom row of Figure 7).

343 The forcing of the QBO and the QBO itself in Figure 7 is concentrated in the deep
 344 tropics, and we now distill the relative alignment of the QBO and its forcing by com-
 345 puting the deep-tropical (4S-4N) averaged wave forcing due to resolved and gravity waves
 346 for this integration and QBO phase (Figure 8a). The tropical zonal winds are shown in
 347 black. Both the resolved and parameterized waves are crucial in providing a westerly torque
 348 in the shear zone below the maximum westerlies, and hence allow for the downward prop-
 349 agation of the westerlies. Furthermore, both resolved and parameterized waves provide
 350 an easterly torque above the maximum westerlies. This vertically oriented dipole in mo-
 351 mentum forcing supports the downward propagation of the QBO winds as the flux pro-
 352 vided by waves is localized within the QBO shear zone.

353 Figure 8b is as in Figure 8a but for the T42L120 integration. In contrast to Fig-
 354 ure 8a, the westerly torque is evident throughout the lower stratosphere and not just in
 355 the shear zones, and the resolved wave forcing in particular peaks far from the shear zone.
 356 The net wave forcing is more effectively canceled out by the vertical advection term ($w*$
 357 $\frac{\partial u}{\partial z}$; not shown) leading to slow downward propagation and a longer period. The key point
 358 of Figure 8 is that for simulations with relatively short QBO periods (Figure 8a), the mo-
 359 mentum flux convergence is concentrated in the shear zones, while for simulations with
 360 longer QBO periods (Figure 8b), the flux is spread out in the vertical over a much broader
 361 region. This effect is even more pronounced for resolved wave forcing than parameter-
 362 ized GW, and the net effect is that the wave forcing is less effective at propagating the
 363 QBO downwards.

In order to consider this effect for all simulations we have performed, we compute the difference in total wave forcing between the westerly shear zone (63hPa to 41hPa, orange line on Figure 8) and the region above the QBO maximum (34hPa to 20hPa, purple line on Figure 8). We then compare this differential zonal momentum either side of 41hPa to the QBO periodicity in Figure 9, with each simulation shown with a distinct marker. This figure includes not only the simulations discussed earlier in this paper, but also the experiments included in Garfinkel et al. (2020a) and Garfinkel et al. (2020b). These two diagnostics are significantly correlated with each other (correlation of -0.62), whereby simulations with stronger westerly forcing in the westerly shear zone simulate a faster downward propagation and subsequently a shorter period. Results are similar if we average over a narrower or broader region on either side of the QBO wind maximum (not shown). The corresponding correlation for the easterly QBO regime is also statistically significant though weaker (correlation is 0.43, plot not shown).

The period of the QBO decreases when all tropospheric stationary waves are removed (Supplemental Figure 1c) in part due to a weakened Brewer-Dobson Circulation (BDC) and hence weaker tropical upwelling. Indeed, the correlation between \bar{w}^* from 4S to 4N at 27hPa with the QBO period for the integrations shown in Figure 9 is 0.34, whereby stronger upwelling leads to a longer period². While this relationship is statistically significant, the variance in periodicity associated with the BDC is much weaker than that associated with resolution, and hence the BDC strength is not the determining factor for QBO period across all of our simulations. Indeed, if we focus on integrations at T42L40 with the gravity wave settings of CONTROL (and include all of the simulations of Garfinkel et al. (2020a) and Garfinkel et al. (2020b)), the correlation is essentially unchanged (correlation of 0.29).

4.3 Explaining the QBO downward propagation

We now turn our attention to understanding the diversity of downward propagation into the lower stratosphere. Figure 4ij and Supplemental Figure 3 showed that a stronger flux of gravity waves leads to a more vigorous QBO with stronger downward

² Note that the BDC depends not only on stationary waves, but also on equatorial waves (which strengthen in these simulations) and also baroclinicly generated synoptic waves in midlatitudes (Jucker & Gerber, 2017; Grise & Thompson, 2013).

propagation, and we now test the hypothesis that stronger resolved wave power also leads to a stronger QBO. We quantify the role of resolved waves for the downward propagation using the total power at 200hPa (below the base of the QBO) associated with variability between $10m/s$ and $20m/s$ for each simulation. We choose this range of power as we expect these waves to be most crucial for downward propagation in the lower stratosphere where winds are weak, though results are similar if we examine, say, $5m/s$ to $15m/s$ or $5m/s$ to $20m/s$. Figure 10 compares the standard deviation of zonal winds at 77hPa to this resolved wave power, with each simulation indicated with a marker. There is clearly a significant relationship between the two, and the correlation is 0.54; that is, a stronger wave forcing is associated with a more vigorous QBO. The correlation for the easterly phase speeds between $-10m/s$ and $-20m/s$ is 0.34.

An additional perspective on downward propagation can be obtained by considering the EPFD in the lowermost stratosphere during the QBO regime with strong winds near 40hPa, as we would expect enhanced resolved wave driving in the lowermost stratosphere to encourage downward propagation. Figure 11 considers this effect, and Figure 11a shows the relationship between winds in the shear zone below the QBO wind maximum and the resolved wave driving lower down, for a composite of events with WQBO winds in the lower stratosphere (composite definition as in Figure 8). Specifically, the ordinate shows the resolved wave EPFD near 100hPa, while the abscissa shows the wind anomaly at 77hPa (in the shear zone) lagged by one month (EPFD is related to the time rate of change of zonal winds). There is clearly a strong relationship, and simulations with stronger resolved wave EPFD also simulate a stronger downward propagation to the lower stratosphere. Wave driving by gravity wave is also significantly correlated with downward propagation to the lowermost stratosphere (Figure 11b), however the regression coefficient for gravity waves is a factor of 9 smaller than that for resolved waves, so resolved waves seem to have a larger influence on the downward propagation in the lowermost stratosphere. Hence we conclude that spread in the dissipation of resolved waves leads to the spread in the ability of the QBO to propagate downwards.

5 Discussion and Conclusions

The Quasi-Biennial Oscillation is the dominant mode of variability in the tropical stratosphere, and while the wind anomalies are confined to the tropics, it impacts the atmospheric circulation and composition globally through a variety of mechanisms.

424 Most models participating in various model intercomparison projects have failed to sim-
 425 ulate the QBO, and even the recent CMIP6 and QBOi models that succeed in simulat-
 426 ing a QBO-like oscillation suffer from a wide range of biases in the QBO behavior. The
 427 goal of this work is to provide a “cookbook” as to the sensitivities of the QBO to a range
 428 of processes, so as to enable modeling groups to more efficiently hone their efforts towards
 429 improving properties of the QBO.

430 Table 1 and Figure 4 summarize the sensitivities of the QBO. Finer horizontal res-
 431 olution is shown to lead to faster QBO downward propagation. Finer vertical resolution
 432 is shown to lead to a longer period and to an increased amplitude in the lowermost strato-
 433 sphere. An increase in the order of numerical hyperdiffusion leads to a shorter period
 434 and a stronger amplitude. Enhancing tropospheric stationary waves leads to a weaker
 435 amplitude. A wider gravity wave spectral width at the source level leads to a slower and
 436 a stronger QBO, but the amplitude effect saturates. A stronger gravity wave stress at
 437 the source leads to a faster and stronger QBO. Launching the gravity wave at a higher
 438 level leads to a stronger QBO. While these sensitivities appear robust in our modeling
 439 framework, we suspect that they can only provide qualitative guidance for other mod-
 440 els while the quantitative details may vary. For example, the regression coefficient be-
 441 tween changes in the gravity wave stress at the source and the QBO standard deviation
 442 likely depends on the specific gravity wave parameterization implemented in a given model.

443 These sensitivities are shown to result from the details of the resultant wave-driven
 444 momentum torque in the stratosphere. The period of the QBO is acutely sensitive to
 445 the relative wave-driven torque directly below versus directly above the QBO wind max-
 446 imum, and models that simulate a dipole in total wave-driven torque, with acceleration
 447 below and deceleration above, simulate a faster period (Figure 9). The amplitude of the
 448 QBO is shown to be related to the amount of waves with relevant phase speeds that can
 449 reach the stratosphere. More waves, whether gravity or resolved, lead to a stronger QBO
 450 in the mid-stratosphere (Figure 10 and 11).

451 Many models suffer from a too-weak amplitude bias in the lowermost stratosphere.
 452 Of the various parameters that can be tuned, the only “fix” we identified that does not
 453 simultaneously increase the amplitude in the mid-stratosphere was to increase vertical
 454 resolution. This result is consistent with Giorgetta et al. (2006) and Anstey et al. (2016,
 455 among others) who also find sensitivity of the QBO to vertical resolution. There are other

ways of increasing the amplitude at 77hPa and simultaneously the amplitude higher up, but then a bias in the lower stratosphere is replaced with a bias in the mid-stratosphere; the only way we found to independently modify the amplitude in the lower stratosphere separately from the mid-stratosphere is via vertical resolution.

Without a careful adjustment of the treatment of unresolved gravity waves, the QBO in MiMA does not converge numerically. Namely, increasing the resolution does not lead to a QBO that is more realistic as compared to observations. However the total resolved wave flux, and more importantly the details of where this flux deposits momentum, differs depending on the resolution, and the QBO is sensitive to the total flux and not just the resolved flux. We now demonstrate explicitly how retuning the gravity wave parameterization can lead to an improved QBO, taking the T42L120 CONTROL run as an example. Recall that this integration simulates a realistic downward propagation to the lowermost stratosphere and a reasonable amplitude, but the period is too long. Our goal is to retune the gravity waves so as to lower the period while minimally modifying the amplitude. Specifically, we set B_{eq} to 6.3mPa and c_w in the tropics to 20m/s; both of these changes should lead to a reduction in the period, while their impacts on the amplitude should mostly cancel out (Figure 4). The resultant QBO is shown in Figure 12 (as compared to Figure 3c). It is clear that the QBO period is substantially improved, even as the amplitude is generally the same. This experiment demonstrates how the QBO cookbook provided in this paper can be used to more efficiently tune the QBO.

When run with 40 vertical levels, sigma levels in the lower stratosphere and tropical tropopause layer are at 0.135, 0.112, 0.092, 0.076, 0.062, and 0.051, which leads to a resolution of between 1.1km (if a scale height of 6km is used) and 1.3km (if a scale height of 7km is used). Previous studies using models with such a coarse resolution typically failed to simulate a QBO (Giorgetta et al., 2006; Richter et al., 2014; Anstey et al., 2016; Geller et al., 2016), though Rind et al. (2014) note that such a coarser vertical resolution still enables the spontaneous generation of a QBO, but it fails to propagate down to the lower stratosphere. We speculate that we nevertheless succeed in simulating a QBO because the resolved wave power spectrum in MiMA is stronger than observed at 200hPa (Supplemental Figure 4) and importantly also at 77hPa (Figure 6), and so the resolved wave forcing of the QBO is still reasonable (as quantified in section 4).

A notable exception to the general tendency of models with poor vertical resolution to fail to simulate a QBO-like oscillation comes from the studies of Yao and Jablonowski (2013) and Yao and Jablonowski (2015). They studied the spontaneous development of a QBO-like oscillation in a dry dynamical core with no convection or gravity wave scheme. Their model nevertheless supported a QBO-like oscillation, though the period was too long and the downward propagation did not extend to the lower stratosphere. They found that a spectral dynamical core supported this QBO-like oscillation more than a finite volume dynamical core, and indeed our configuration of MiMA uses a spectral dynamical core.

None of our simulations simulate disruptions as extreme as those that have occurred in the past five years (e.g. near 2016 in Figure 3a), though the simulations with weak QBOs occasionally skip a particular phase and instead simulate a prolonged, e.g., westerly phase (see the $B_{eq} = 0.0023$ simulation near year 30 in Supplemental Figure 3). Hence a disruption can arise spontaneously if there is relatively weak gravity wave flux leaving the troposphere, even as no external perturbations are imposed in the troposphere. While such a mechanism may not be relevant for the disruption in 2015/2016 when wave activity was anomalously strong (Kang et al., 2020), a weakening of the QBO under climate change (Kawatani & Hamilton, 2013; Rao et al., 2020c) may make it more susceptible to disruptions.

Overall, this study shows that a wide range of parameters affect the QBO, and hence we expect that biases in e.g. QBO strength or periodicity can be “fixed” in a comprehensive model by carefully adjusting these parameters in parallel. This effect is demonstrated in Figure 12: Figure 12 shows a remarkably realistic QBO, particularly in terms of its penetration into the lower stratosphere, obtained by enhancing the vertical resolution and adjusting the gravity wave parameterization source spectrum.

6 Appendix: Implementation of a gravity wave scheme in a model of an idealized moist atmosphere (MiMA)

Gravity waves have important global effects on the circulation, temperature structure, and composition of the atmosphere, but occur on spatial scales that are too fine to be resolved by nearly all general circulation models (Alexander et al., 2010). Gravity waves carry momentum and energy vertically in the atmosphere, and they are an important forcing term in the stratospheric momentum budget. Models must parameter-

ize these forcing terms using information on the larger-scale wind and stability fields. Most gravity wave schemes share a few common attributes: a series of waves with various possible combinations of the ground-relative phase speed and horizontal wavenumber are launched, and the dissipation of the waves as a function of height is based on the concepts of “breaking” (Lindzen, 1981) due to the presence of critical lines, and “saturation” (Fritts, 1984; Dunkerton, 1989), as density decreases and gravity wave amplitude grows. We parameterize gravity waves following Alexander and Dunkerton (1999), Donner et al. (2011), and Cohen et al. (2013), and while the criteria for breaking and dissipation of waves is left unchanged, we have modified the properties of the wave source. This appendix documents these changes.

A key parameter in any parameterization of gravity waves is the distribution of stress across phase speeds, and we thus repeat the treatment of this in the parameterization of Alexander and Dunkerton (1999) (their equation 17):

$$B_0(c) = \text{sgn}(\hat{c}) B_m \exp \left[- \left(\frac{c - c_0}{c_w} \right)^2 \ln 2 \right] \quad (1)$$

Here c is the ground-relative phase speed; c_0 is the phase speed with maximum flux magnitude B_m , and in all experiments in this paper $B_m = 0.4 \text{ m}^2/\text{s}^2$; c_w is the half-width at half-maximum of the Gaussian (35 m/s in all integrations poleward of 10S and 10N , and 35 m/s in the tropics as well unless specified otherwise); and \hat{c} is the intrinsic phase speed at source level. The source level is set at 315 hPa in the tropics (following Donner et al., 2011) unless otherwise specified. The spectral resolution for the phase speed bins is 2 m/s , and the tropical wave spectrum is set to be symmetric about the zonal wind at the source level (c_0 is set to the zonal wind), for all integrations shown in this paper.

$B_0(c)$ represents the gravity wave amplitude during an active wave event, however gravity waves are by their very nature intermittent. The parameterization of Alexander and Dunkerton (1999) handles this intermittency by a separate parameter F_{S0} which is intended to represent the long-term average of momentum flux integrated across all phase speeds. F_{S0} and $B_0(c)$ are related by an intermittency factor ϵ following equation 19 of Alexander and Dunkerton (1999) as

$$\epsilon = \frac{F_{S0} \Delta c}{\bar{\rho}_o \sum_c |B_0(c)| \Delta c} \quad (2)$$

The value of F_{S0} in many GW parameterizations is not constant in latitude (Donner et al., 2011; Molod et al., 2012; Anstey et al., 2016), and we explore the importance of

548 latitudinal dependence in F_{S0} as described in Equation 3:

$$F_{S0}(\phi) = \begin{cases} Bt_0 + 0.5Bt_{SH}(1. + \tanh(\frac{\phi - \phi_{0s}}{\delta\phi_s})) & , \quad \phi \leq \phi_{0s} \\ Bt_0 + \frac{Bt_{eq} - Bt_0}{\phi_{0s} - \delta\phi_s}(\phi_{0s} - \phi) & , \quad \phi_{0s} \leq \phi < \delta\phi_s \\ Bt_{eq} & , \quad \delta\phi_s \leq \phi \leq \delta\phi_n \\ Bt_0 + \frac{Bt_{eq} - Bt_0}{\phi_{0n} - \delta\phi_n}(\phi_{0n} - \phi) & , \quad \delta\phi_n < \phi \leq \phi_{0n} \\ Bt_0 + 0.5Bt_{NH}(1. + \tanh(\frac{\phi - \phi_{0n}}{\delta\phi_n})) & , \quad \phi \geq \phi_{0n} \end{cases} \quad (3)$$

549 In CONTROL, $Bt_0 = 0.0043\text{Pa}$, and $Bt_{eq} = Bt_0 = 0.0043$, such that the same stress
 550 is imposed in both the tropics and subtropics, but we explore sensitivity to Bt_{eq} . Ad-
 551 dditional stress is included in midlatitudes and subpolar latitudes by setting $Bt_{NH} = 0.0035\text{Pa}$
 552 and $Bt_{SH} = 0.0035\text{Pa}$; this extra drag helps to keep the polar vortex from becoming
 553 too strong. Note that we do not include any orographic gravity wave drag in our model
 554 setup. Finally, $\phi_{0n} = 15^\circ$, $\phi_{0s} = -15^\circ$, $\delta\phi_n = 10^\circ$, $\delta\phi_s = -10^\circ$ specify the meridional ex-
 555 tent of the QBO, and are also unchanged in all of our experiments. This functional form
 556 loosely follows a similar form in the GEOSCCM model and MERRA-2 reanalysis (Figure
 557 5 of Molod et al., 2012) and the Canadian Middle Atmosphere Model (CMAM, Anstey
 558 et al., 2016). The net effect of this change is that the intermittency factor ϵ is made a
 559 function of latitude, and specifically gravity waves are more frequently present in mid-
 560 latitudes, and also in the tropics if Bt_{eq} is larger than Bt_0 .

561 An additional change made from the configuration in Alexander and Dunkerton
 562 (1999) and Cohen et al. (2013) is that the momentum associated with gravity waves that
 563 would leave the upper model domain is deposited evenly in the levels above 0.85hPa in
 564 order to conserve momentum. (There are three such levels when the model is run with
 565 40 total levels.) This avoids any complications noted by Shepherd and Shaw (2004) and
 566 Shaw and Shepherd (2007) associated with non-conservation of momentum. Note that
 567 Cohen et al. (2013) inserted this momentum evenly in the levels above 0.5hPa. No sponge
 568 layer is included in the model.

569 Acknowledgments

570 CIG, EPG, OS, JR, IPW, and NP are supported by a European Research Council start-
 571 ing grant under the European Unions Horizon 2020 research and innovation programme
 572 (grant agreement No 677756). EPG acknowledges further support from the US NSF through
 573 grant AGS 1852727. MJ acknowledges support from the Australian Research Council
 574 (ARC) Centre of Excellence for Climate Extremes (CE170100023). Correspondence should

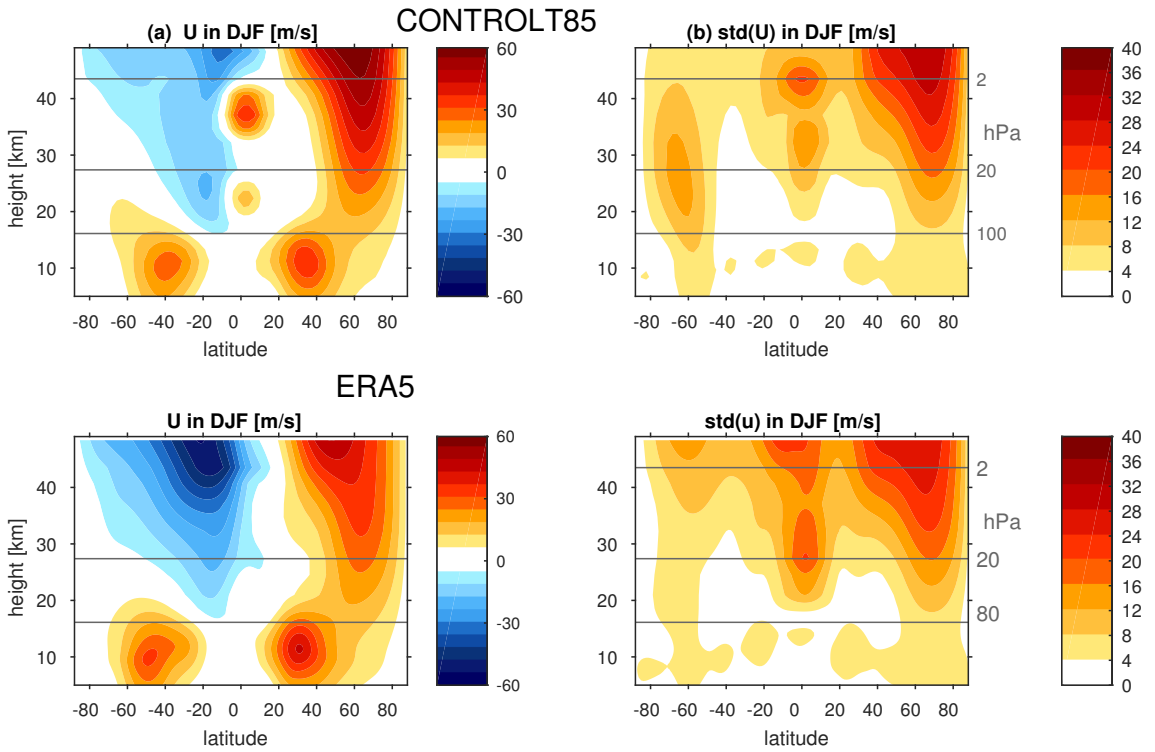


Figure 1. (a) Zonal mean zonal wind climatology in December through February; (b) standard deviation of the zonally averaged zonal wind. For (a), the contour interval is 6 m/s and the 0 m/s contour is omitted. (top) in Control at T85 with 40 vertical levels; (bottom) in ERA5

	List of simulations in this paper		
	std dev 20hPa	std dev 77hPa	period 27hPa
ERA-5	17.9	4.5	2.4
CONTROL	14.9	3.3	2.5
CONTROL 120 levels	14.5	5.5	4.1
CONTROL 30 level	14.4	2.7	2.0
CONTROL, T85	16.9	3.0	1.2
CONTROL, T63	18.3	3.8	1.8
CONTROL, nabla6	12.1	3.2	2.5
CONTROL, nabla10	19.3	4.2	2.2
zonally symmetric BC	23.9	4.9	2.3
CONTROL, cw=45	15.5	3.5	2.5
CONTROL, cw=25	13.8	2.9	2.5
CONTROL, cw=15	8.9	2.4	2.1
CONTROL, cw=5	3.7	2.1	1.0
CONTROL, $B_{eq}=0.0063$	22.5	5.1	2.0
CONTROL, $B_{eq}=0.0023$	10.0	2.2	2.4
CONTROL, $B_{eq}=0.0013$	5.6	2.2	2.3
CONTROL, launch=150hPa, cw=25	16.5	3.4	2.4

Figure 2. A list of experiments included in this paper, with color shading added for clarity.

Note that in addition to these 16 simulations, the scatter plots show additional integrations used in Garfinkel et al. (2020a) and Garfinkel et al. (2020b). Experiment 1 was performed at T42 with 40 vertical levels, ∇^8 hyperdiffusion, $cw=35\text{m/s}$, $B_{eq}=0.0043\text{Pa}$, and a launch height of 315hPa, and the other experiments use these settings except as otherwise specified. For ERA-5, the standard deviation at 80hPa is shown instead of 77hPa, and the period is computed at 30hPa instead of 27hPa. Note that while the T42L40 simulations simulate too weak a standard deviation at 20hPa, they simulate too strong a standard deviation at 10hPa.

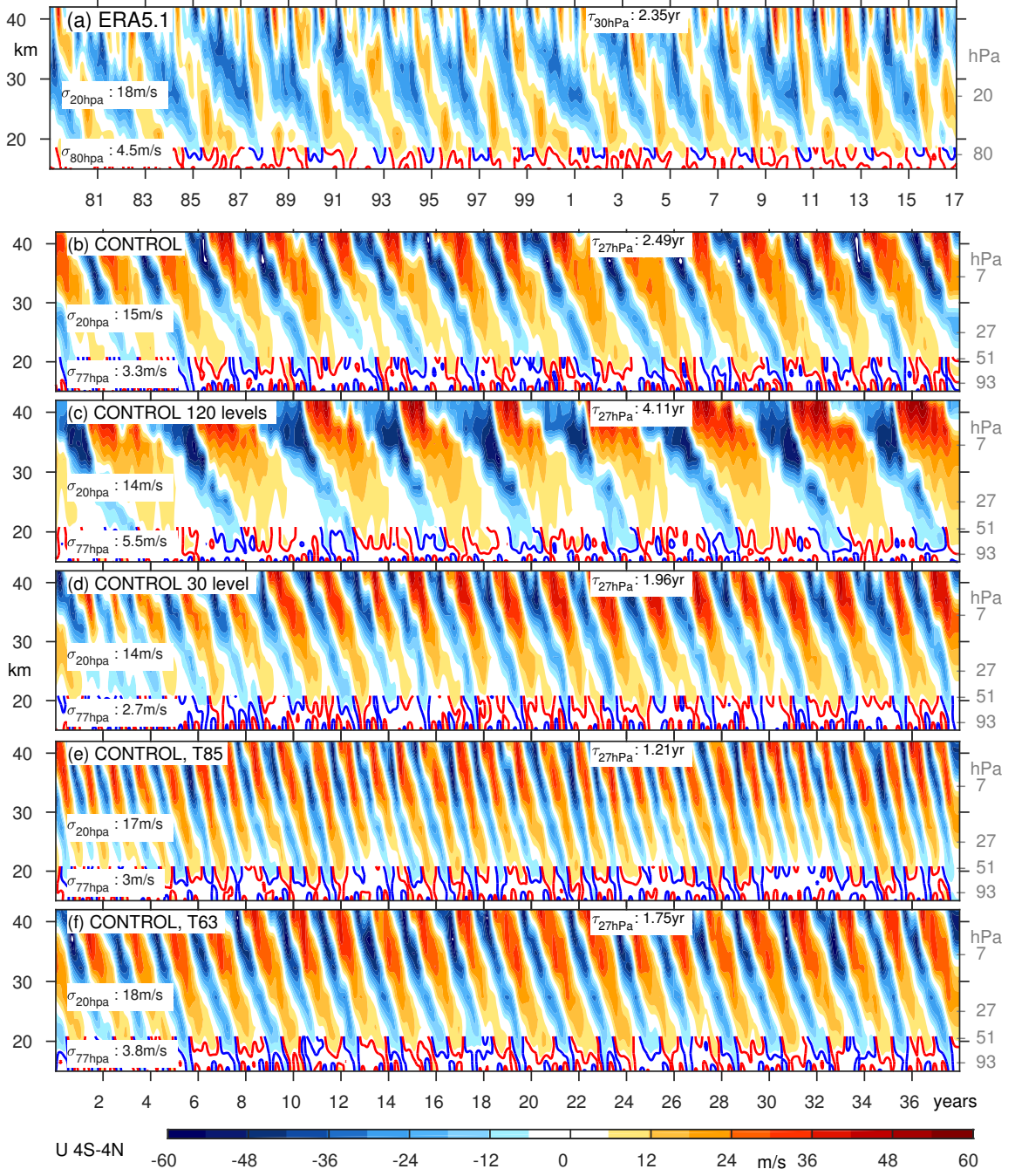


Figure 3. Zonal mean zonal wind from 4S-4N in (a) ERA5, (b) Control at T42 with 40 vertical levels; (c) Control at T42 with 120 vertical levels; (d) Control at T42 with 30 vertical levels; (e) Control at T85 with 40 vertical levels; (e) Control at T63 with 40 vertical levels. Each panel indicates the standard deviation of winds at 20hPa and 77hPa, and the period at 27hPa. The contour interval is 6m/s, and the 3m/s contour is shown in blue and red in the lower stratosphere.

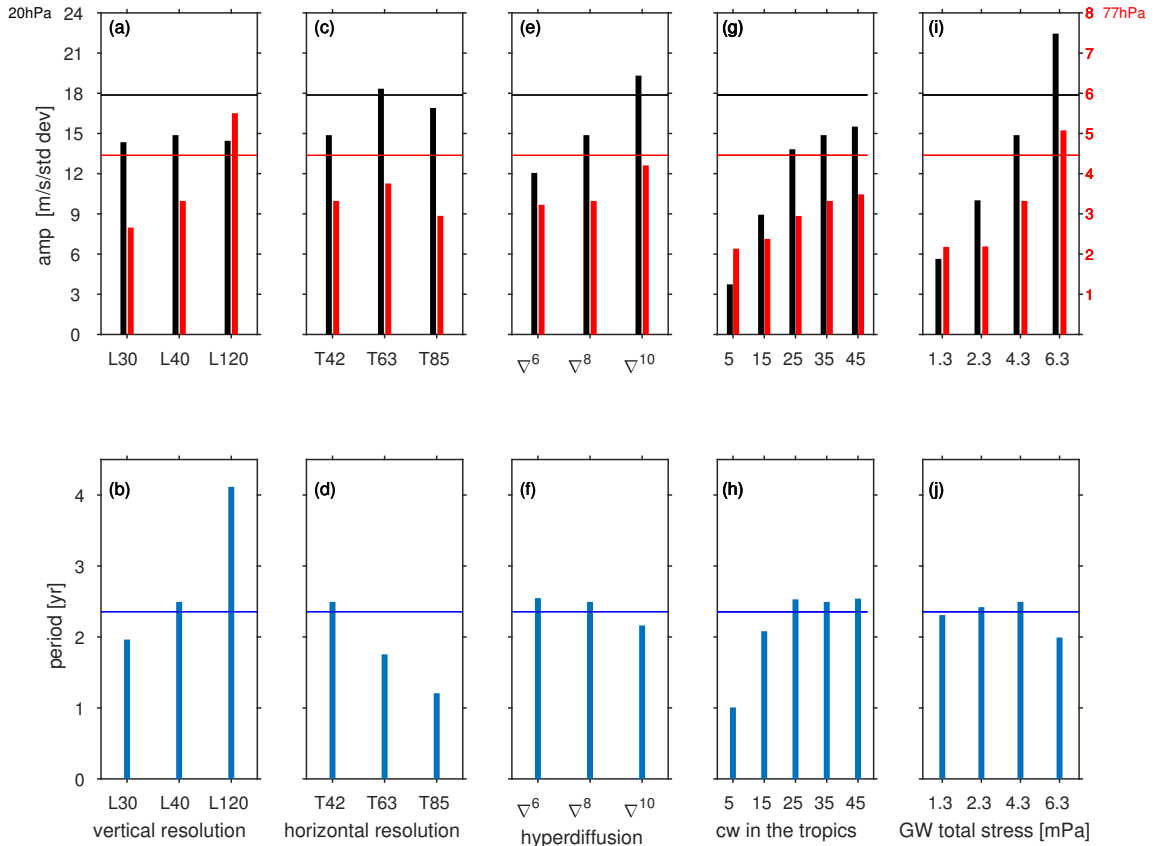


Figure 4. Summary of the sensitivities of the QBO period and amplitude to (a-b) vertical resolution; (c-d) horizontal resolution; (e-f) hyperdiffusion order; (g-h) spectral width of the launched gravity waves in the tropics; (i-j) total gravity wave stress in the tropics. A horizontal line denotes the corresponding value from ERA-5.

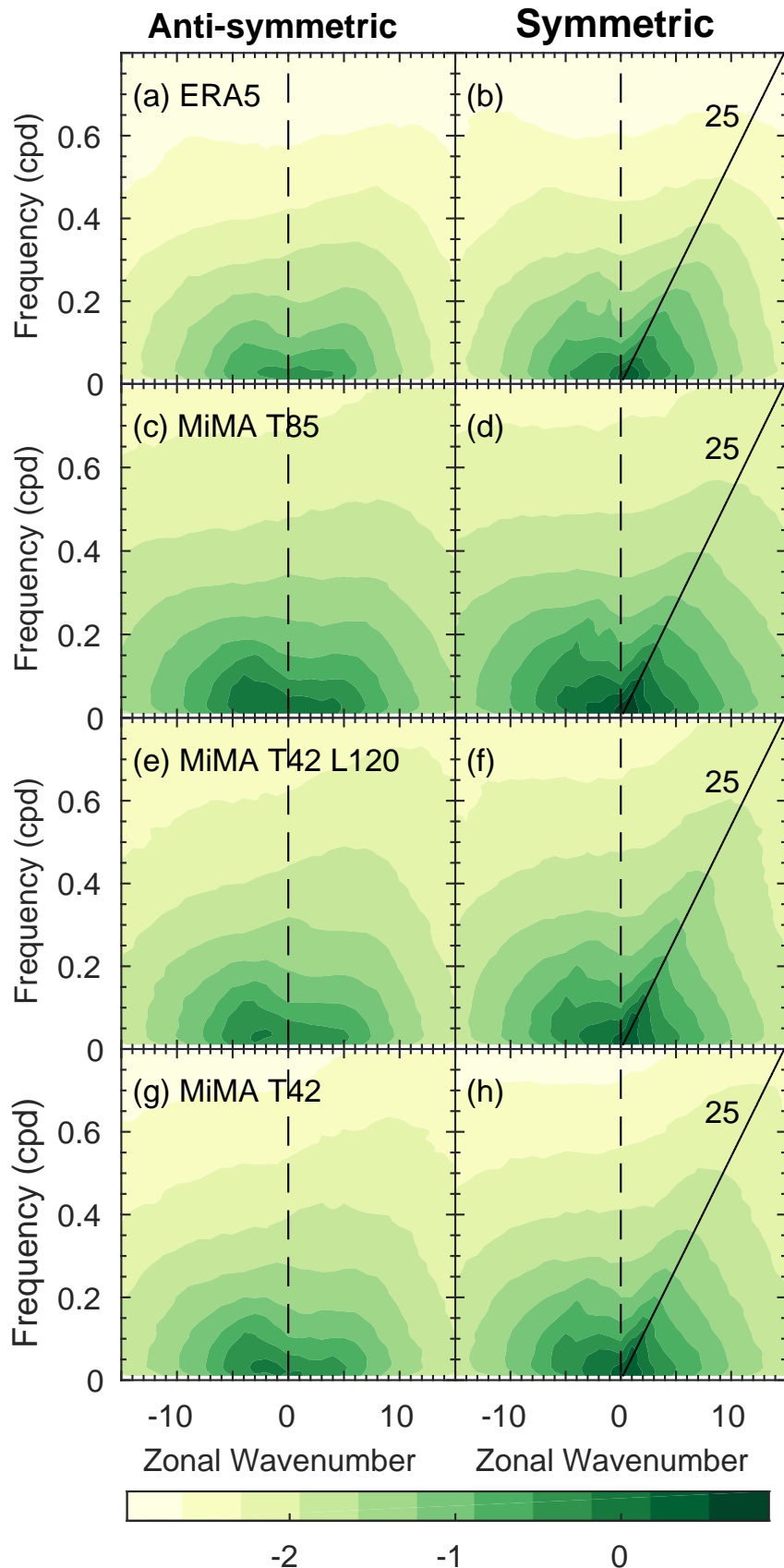
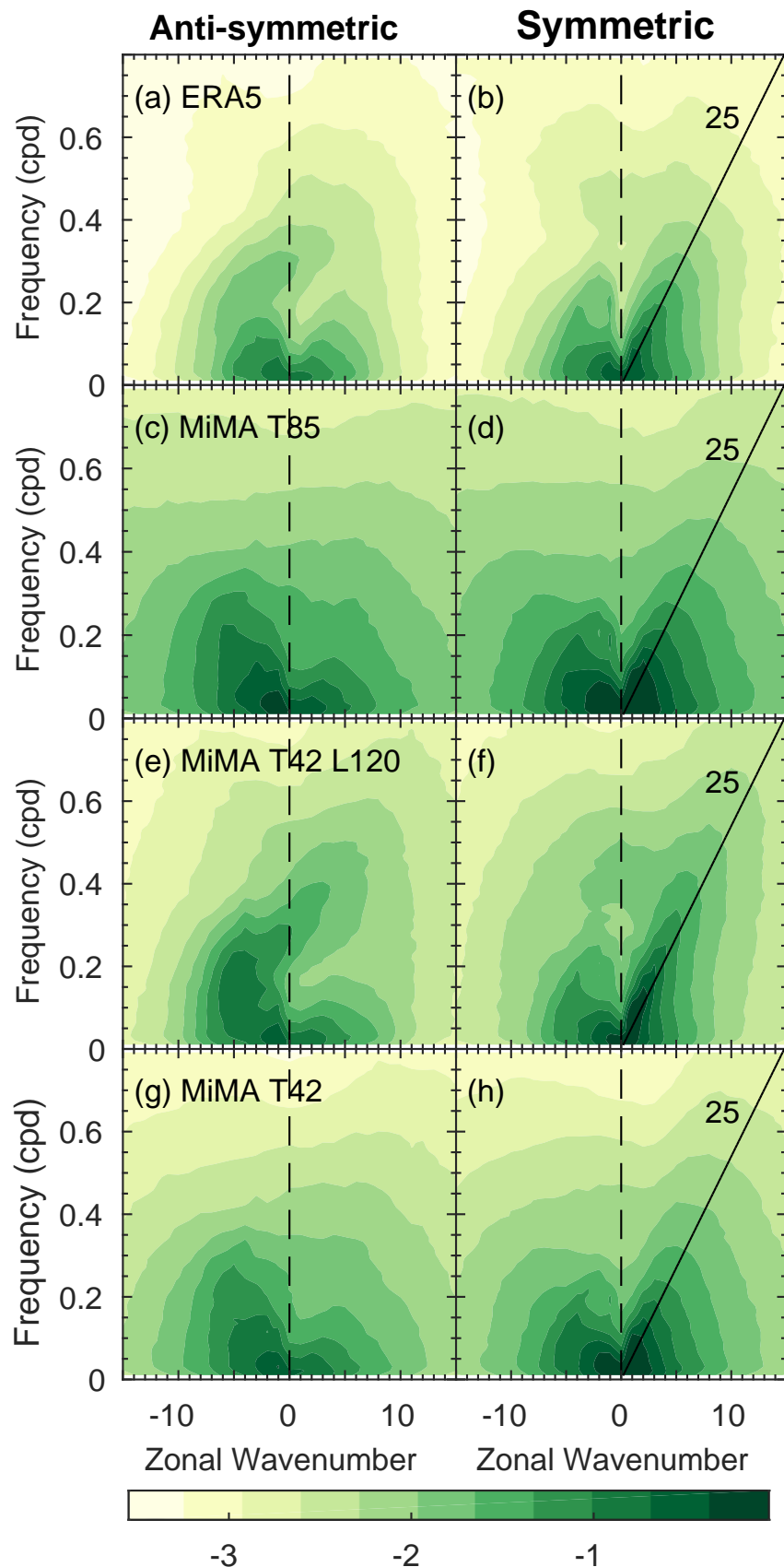


Figure 5. The logarithm base-10 of the raw symmetric and anti-symmetric spectrum of zonal wind at 200hPa from 15S to 15N in (a-b) ERA5; (c-d) Control at T85 with 40 vertical levels; (e-f) Control at T42 with 120 vertical levels; (g-h) Control at T42 with 40 vertical levels.

**Figure 6.** As in Figure 5 but for 77hPa.

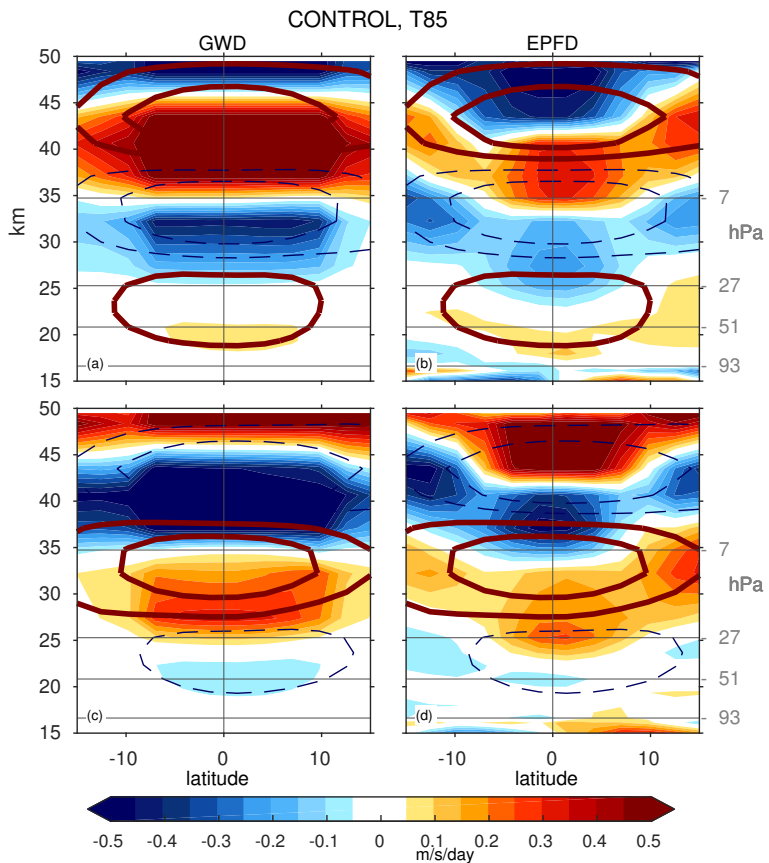


Figure 7. Forcing of winds by (left) parameterized gravity waves and (right) resolved waves for CONTROL at T85 for a QBO phase defined as wind anomalies at 41hPa between (top) 10m/s and 15m/s (i.e. WQBO) and (bottom) -10m/s and -15m/s (i.e. EQBO). Results are similar for other resolutions (not shown).

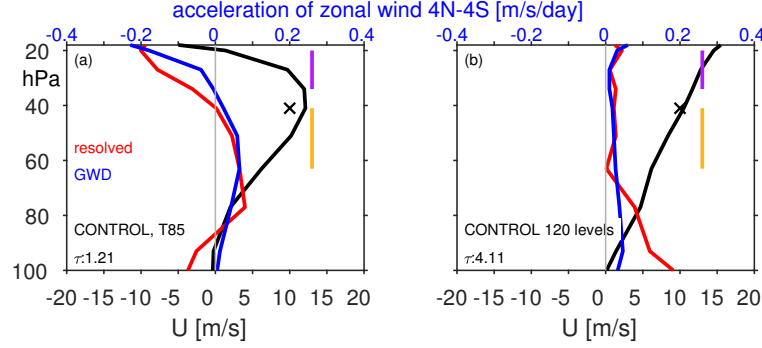


Figure 8. QBO and its resolved and parameterized wave forcing in integrations with a relatively (left) fast period and (right) slow period for a WQBO composite in which anomalous zonal winds at 41hPa must be between 10 and 15m/s. The x-axis for the QBO is shown on the bottom, and for the wave forcings on the top. Orange and purple lines show regions averaged over for Figure 9.

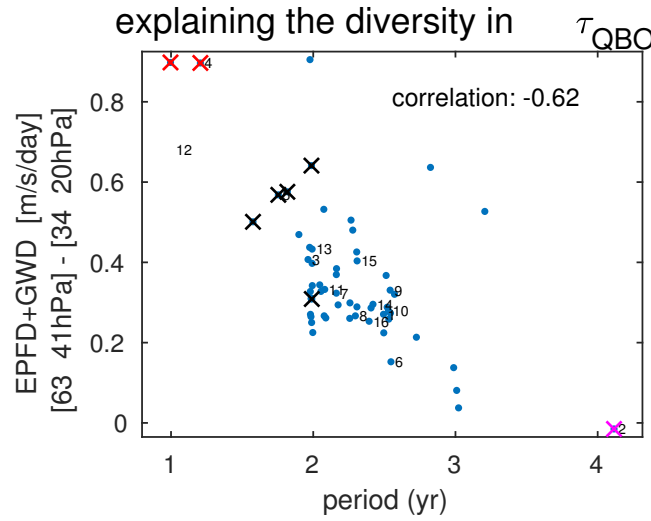


Figure 9. Relationship between QBO periodicity and the difference in total wave driving on either side of the winds at 41hPa (see orange and purple lines in Figure 8), for a WQBO composite in which anomalous zonal winds at 41hPa must be between 10 and 15m/s. Numbering of experiments follows Figure 2, and additional experiments performed as part of Garfinkel et al. (2020b) and Garfinkel et al. (2020a) are shown unnumbered for clarity. Black x-es correspond to runs at T63, red x-es to runs at T85, and magenta to runs with 120 levels.

Table 1. summary of the sensitivities of the QBO

Table: summary of the QBO's sensitivities

	period	amplitude
finer horizontal resolution	faster	small effect
finer vertical resolution	slower	stronger but only in lowermost stratosphere
higher hyperdiffusion power	faster	stronger
adding tropospheric stationary waves	small effect	weaker
wider gravity wave spectral width	slower	stronger, but effect saturates
stronger gravity wave amplitude	faster	stronger
higher gravity wave launch level	small effect	stronger

be addressed to C.I.G. (email: chaim.garfinkel@mail.huji.ac.il). The source code for the model configuration used in this study will be available on GitHub as part of MiMAv2.0.

References

- Alexander, M., & Dunkerton, T. (1999). A spectral parameterization of mean-flow forcing due to breaking gravity waves. *Journal of the atmospheric sciences*, 56(24), 4167–4182. doi: 10.1175/1520-0469(1999)056<4167:ASPOMF>2.0.CO;2
- Alexander, M., Geller, M., McLandress, C., Polavarapu, S., Preusse, P., Sassi, F., ... Watanabe, S. (2010). Recent developments in gravity-wave effects in climate models and the global distribution of gravity-wave momentum flux from observations and models. *Quarterly Journal of the Royal Meteorological Society*, 136(650), 1103–1124. Retrieved from <https://rmets.onlinelibrary.wiley.com/doi/abs/10.1002/qj.637> doi: <https://doi.org/10.1002/qj.637>
- Anstey, J. A., Scinocca, J. F., & Keller, M. (2016). Simulating the qbo in an atmospheric general circulation model: Sensitivity to resolved and parameterized forcing. *Journal of the Atmospheric Sciences*, 73(4), 1649–1665.
- Anstey, J. A., & Shepherd, T. G. (2014). High-latitude influence of the quasi-biennial oscillation. *Quarterly Journal of the Royal Meteorological Society*,

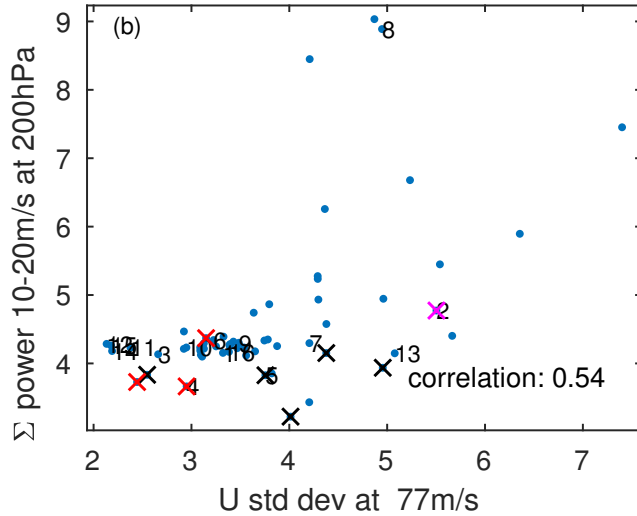


Figure 10. Relationship between QBO standard deviation at 77hPa and the resolved wave driving at 200hPa between 10m/s and 20m/s. The resolved wave driving in this range can be computed by summing over the appropriate spectral bins in, say, Figure 5. Numbering of experiments follows Figure 2, and additional experiments performed as part of Garfinkel et al. (2020b) and Garfinkel et al. (2020a) are shown unnumbered for clarity.

594

140(678), 1–21.

595

Baldwin, M. P., Gray, L. J., Dunkerton, T. J., Hamilton, K., Haynes, P. H., Randall, W. J., ... Takahashi, M. (2001). The Quasi-Biennial Oscillation. *Rev. Geophys.*, 39(2), 179–229.

598

Betts, A., & Miller, M. (1986). A new convective adjustment scheme. part ii: Single column tests using gate wave, bomex, atex and arctic air-mass data sets. *Quarterly Journal of the Royal Meteorological Society*, 112(473), 693–709. doi: 10.1002/qj.49711247308

600

Betts, A. K. (1986). A new convective adjustment scheme. part i: Observational and theoretical basis. *Quarterly Journal of the Royal Meteorological Society*, 112(473), 677–691. doi: 10.1002/qj.49711247307

601

Bushell, A., Anstey, J., Butchart, N., Kawatani, Y., Osprey, S., Richter, J., ... others (2020). Evaluation of the quasi-biennial oscillation in global climate models for the sparc qbo-initiative. *Quarterly Journal of the Royal Meteorological Society*.

602

Butchart, N., Anstey, J., Hamilton, K., Osprey, S., McLandress, C., Bushell, A.,

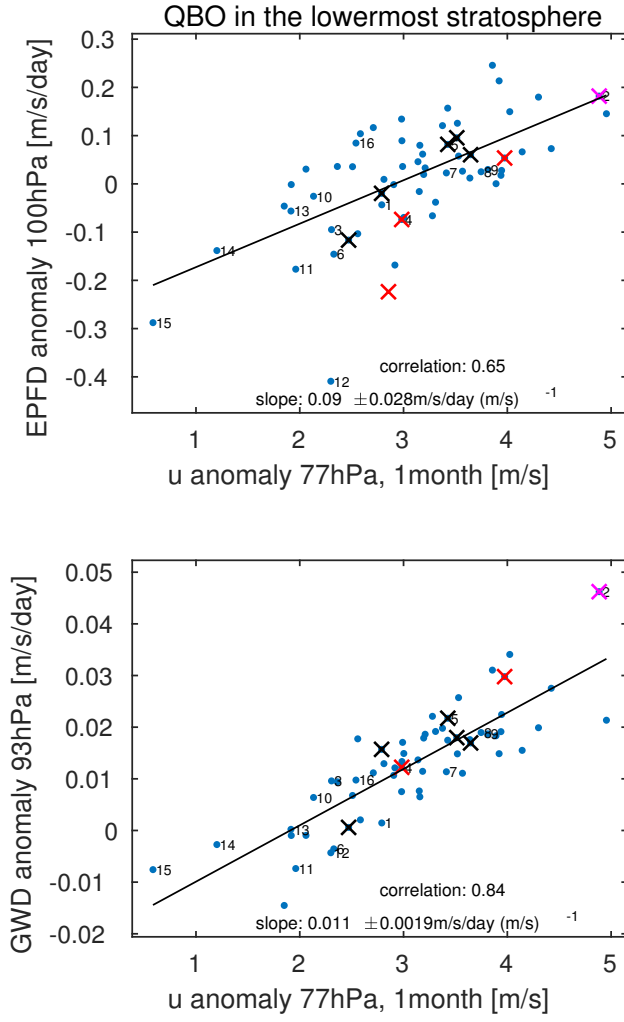


Figure 11. Relationship between winds in the shear zone below the QBO wind max and the wave driving lower down, for a WQBO composite in which anomalous zonal winds at 41hPa must be between 10 and 15m/s. Numbering of experiments follows Figure 2, and additional experiments performed as part of Garfinkel et al. (2020b) and Garfinkel et al. (2020a) are shown unnumbered for clarity.

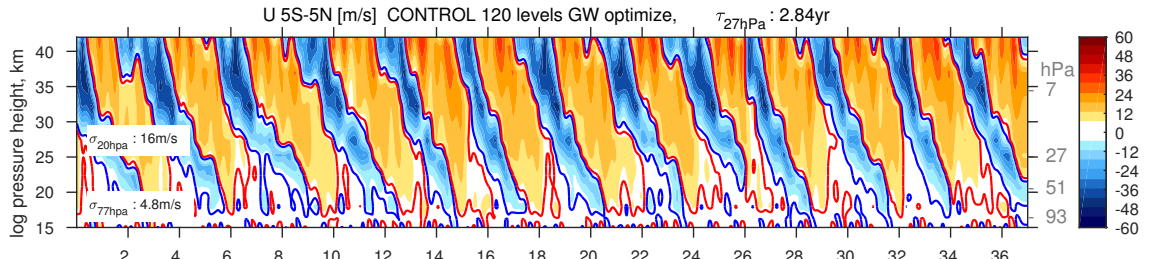


Figure 12. QBO in a T42L120 run in which the gravity wave settings have been modified to improve the QBO periodicity. Specifically B_{eq} is set to 6.3mPa and c_w in the tropics to 20m/s.

- ... others (2018). Overview of experiment design and comparison of models participating in phase 1 of the sparc quasi-biennial oscillation initiative (qboi). *Geoscientific Model Development*, 11(3).
- Cohen, N. Y., Gerber, E. P., & Oliver Bühler, E. P. (2013). Compensation between resolved and unresolved wave driving in the stratosphere: Implications for downward control. *Journal of the Atmospheric Sciences*, 70(12), 3780–3798. doi: 10.1175/JAS-D-12-0346.1
- Collimore, C. C., Martin, D. W., Hitchman, M. H., Huesmann, A., & Waliser, D. E. (2003). On the relationship between the QBO and tropical deep convection. *J. Clim.*, 16(15). doi: 10.1175/1520-0442(2003)
- Diallo, M., Riese, M., Birner, T., Konopka, P., Muller, R., Hegglin, M. I., ... Ploeger, F. (2018). Response of stratospheric water vapor and ozone to the unusual timing of el niño and the qbo disruption in 2015–2016. *Atmospheric Chemistry and Physics*, 18(17), 13055–13073.
- Donner, L. J., Wyman, B. L., Hemler, R. S., Horowitz, L. W., Ming, Y., Zhao, M., ... Zeng, F. (2011). The dynamical core, physical parameterizations, and basic simulation characteristics of the atmospheric component am3 of the gfdl global coupled model cm3. *Journal of Climate*, 24(13). doi: 10.1175/2011JCLI3955.1
- Dunkerton, T. J. (1989). Theory of internal gravity wave saturation. In *Middle atmosphere* (pp. 373–397). Springer.
- Ern, M., Ploeger, F., Preusse, P., Gille, J., Gray, L., Kalisch, S., ... Riese, M. (2014). Interaction of gravity waves with the qbo: A satellite perspective.

- 633 *Journal of Geophysical Research: Atmospheres*, 119(5), 2329–2355. doi:
 634 10.1002/2013JD020731
- 635 Frierson, D. M., Held, I. M., & Zurita-Gotor, P. (2006). A gray-radiation aquaplanet
 636 moist gcm. part i: Static stability and eddy scale. *Journal of the atmospheric*
 637 *sciences*, 63(10), 2548–2566. doi: 10.1175/JAS3753.1
- 638 Frierson, D. M., Held, I. M., & Zurita-Gotor, P. (2007). A gray-radiation aquaplanet
 639 moist gcm. part ii: Energy transports in altered climates. *Journal of the atmos-*
 640 *spheric sciences*, 64(5), 1680–1693. doi: 10.1175/JAS3913.1
- 641 Fritts, D. C. (1984). Gravity wave saturation in the middle atmosphere: A review of
 642 theory and observations. *Reviews of Geophysics*, 22(3), 275–308.
- 643 Garfinkel, C. I., & Hartmann, D. L. (2011a). The influence of the Quasi-Biennial
 644 Oscillation on the troposphere in wintertime in a hierarchy of models, part
 645 1-simplified dry GCMs. *J. Atmos. Sci.*, 68. doi: 10.1175/2011JAS3665.1
- 646 Garfinkel, C. I., & Hartmann, D. L. (2011b). The influence of the Quasi-
 647 Biennial Oscillation on the troposphere in wintertime in a hierarchy of
 648 models, part 2- perpetual winter WACCM runs. *J. Atmos. Sci.*, 68. doi:
 649 10.1175/2011JAS3701.1
- 650 Garfinkel, C. I., Shamir, O., Fouxon, I., & Paldor, N. (2021). Tropical background
 651 and wave spectra: contribution of wave-wave interactions in a moderately
 652 nonlinear turbulent flow. *Journal of the Atmospheric Sciences*, in press. Re-
 653 trieved from <https://journals.ametsoc.org/view/journals/atsc/aop/JAS-D-20-0284.1/JAS-D-20-0284.1.xml> doi: 10.1175/JAS-D-20-0284.1
- 655 Garfinkel, C. I., Shaw, T. A., Hartmann, D. L., & Waugh, D. W. (2012). Does the
 656 holton-tan mechanism explain how the quasi-biennial oscillation modulates the
 657 arctic polar vortex? *Journal of the Atmospheric Sciences*, 69(5), 1713–1733.
 658 doi: 10.1175/JAS-D-11-0209.1
- 659 Garfinkel, C. I., White, I., Gerber, E. P., & Jucker, M. (2020b). The impact of sst
 660 biases in the tropical east pacific and agulhas current region on atmospheric
 661 stationary waves in the southern hemisphere. *Journal of Climate*, 33(21),
 662 9351–9374.
- 663 Garfinkel, C. I., White, I. P., Gerber, E. P., & Jucker, M. (2020a). The building
 664 blocks of northern hemisphere wintertime stationary waves. *Journal of Cli-*
 665 *mate*, 33(13). doi: 10.1175/JCLI-D-19-0181.1

- 666 Geller, M. A., Zhou, T., Shindell, D., Ruedy, R., Aleinov, I., Nazarenko, L., ... oth-
 667 ers (2016). Modeling the qbo-improvements resulting from higher-model
 668 vertical resolution. *Journal of advances in modeling earth systems*, 8(3),
 669 1092–1105.
- 670 Giorgetta, M., Manzini, E., Roeckner, E., Esch, M., & Bengtsson, L. (2006). Cli-
 671 matology and forcing of the quasi-biennial oscillation in the maecham5 model.
 672 *Journal of Climate*, 19(16), 3882–3901.
- 673 Grise, K. M., & Thompson, D. W. J. (2013). On the signatures of equatorial and
 674 extratropical wave forcing in tropical tropopause layer temperatures. *J. Atmos.*
 675 *Sci.*, 70, 1084–1102. doi: 10.1175/JAS-D-12-0163.1
- 676 Gupta, A., Gerber, E. P., & Lauritzen, P. H. (2020). Numerical impacts on tracer
 677 transport: A proposed intercomparison test of atmospheric general circula-
 678 tion models. *Quarterly Journal of the Royal Meteorological Society*, 146(733),
 679 3937–3964.
- 680 Hamilton, K., Wilson, R. J., & Hemler, R. S. (2001). Spontaneous stratospheric qbo-
 681 like oscillations simulated by the gfdl skyhi general circulation model. *Journal*
 682 *of the atmospheric sciences*, 58(21), 3271–3292.
- 683 Hersbach, H., Bell, B., Berrisford, P., Hirahara, S., Horányi, A., Muñoz-Sabater, J.,
 684 ... others (2020). The era5 global reanalysis. *Quarterly Journal of the Royal*
 685 *Meteorological Society*, 146(730), 1999–2049.
- 686 Holt, L. A., Alexander, M., Coy, L., Molod, A., Putman, W., & Pawson, S. (2016).
 687 Tropical waves and the quasi-biennial oscillation in a 7-km global climate
 688 simulation. *Journal of the Atmospheric Sciences*, 73(9), 3771–3783.
- 689 Holt, L. A., Lott, F., Garcia, R. R., Kiladis, G. N., Cheng, Y.-M., Anstey, J. A., ...
 690 Yukimoto, S. (2020). An evaluation of tropical waves and wave forcing of the
 691 qbo in the qboi models. *Quarterly Journal of the Royal Meteorological Society*,
 692 n/a(n/a). Retrieved from <https://rmets.onlinelibrary.wiley.com/doi/abs/10.1002/qj.3827> doi: <https://doi.org/10.1002/qj.3827>
- 694 Holton, J. R., & Lindzen, R. S. (1972). An updated theory for the quasi-biennial
 695 cycle of the tropical stratosphere. *Journal of the Atmospheric Sciences*, 29(6),
 696 1076–1080.
- 697 Holton, J. R., & Tan, H. C. (1980). The influence of the equatorial Quasi-Biennial
 698 Oscillation on the global circulation at 50mb. *J. Atmos. Sci.*, 37, 2200–2208.

- 699 Iacono, M. J., Mlawer, E. J., Clough, S. A., & Morcrette, J.-J. (2000). Impact of
 700 an improved longwave radiation model, rrtm, on the energy budget and ther-
 701 modynamic properties of the ncar community climate model, ccm3. *Journal of*
 702 *Geophysical Research: Atmospheres*, 105(D11), 14873–14890.
- 703 Jucker, M., & Gerber, E. (2017). Untangling the annual cycle of the tropical
 704 tropopause layer with an idealized moist model. *Journal of Climate*, 30(18),
 705 7339–7358.
- 706 Kang, M.-J., Chun, H.-Y., & Garcia, R. R. (2020). Role of equatorial waves and
 707 convective gravity waves in the 2015/16 quasi-biennial oscillation disruption.
 708 *Atmospheric Chemistry and Physics*, 20(23), 14669–14693.
- 709 Kawatani, Y., & Hamilton, K. (2013). Weakened stratospheric quasibiennial oscilla-
 710 tion driven by increased tropical mean upwelling. *Nature*, 497(7450), 478–481.
 711 doi: 10.1038/nature12140
- 712 Kiladis, G. N., Wheeler, M. C., Haertel, P. T., Straub, K. H., & Roundy, P. E.
 713 (2009). Convectively coupled equatorial waves. *Reviews of Geophysics*, 47(2).
- 714 Liess, S., & Geller, M. A. (2012). On the relationship between qbo and distribu-
 715 tion of tropical deep convection. *J. Geophys. Res.*, 117(D03108). doi: 10.1029/
 716 2011JD016317
- 717 Lindzen, R. S. (1981). Turbulence and stress owing to gravity wave and tidal
 718 breakdown. *Journal of Geophysical Research: Oceans*, 86(C10), 9707–9714.
 719 Retrieved from <https://agupubs.onlinelibrary.wiley.com/doi/abs/10.1029/JC086iC10p09707> doi: <https://doi.org/10.1029/JC086iC10p09707>
- 721 Lindzen, R. S., & Holton, J. R. (1968). A theory of the quasi-biennial oscillation.
 722 *Journal of the Atmospheric Sciences*, 25(6), 1095–1107.
- 723 Manzini, E., Giorgetta, M. A., Kornbluth, L., & Roeckner, E. (2006). The influence
 724 of sea surface temperatures on the northern winter stratosphere: Ensemble
 725 simulations with the MAECHAM5 model. *J. Clim.*, 19, 3863–3881.
- 726 Martin, Z., Wang, S., Nie, J., & Sobel, A. (2019). The impact of the qbo on mjo
 727 convection in cloud-resolving simulations. *Journal of the Atmospheric Sci-
 728 ences*, 76(3), 669–688.
- 729 Matsuno, T. (1966). Quasi-geostrophic motions in the equatorial area. *Journal*
 730 *of the Meteorological Society of Japan. Ser. II*, 44(1), 25–43. doi: https://doi.org/10.2151/jmsj1965.44.1_25

- 732 Merlis, T. M., Schneider, T., Bordoni, S., & Eisenman, I. (2013). Hadley circulation
 733 response to orbital precession. part ii: Subtropical continent. *Journal of Climate*, 26(3), 754–771.
- 734
- 735 Mlawer, E. J., Taubman, S. J., Brown, P. D., Iacono, M. J., & Clough, S. A.
 736 (1997). Radiative transfer for inhomogeneous atmospheres: Rrtm, a vali-
 737 dated correlated-k model for the longwave. *Journal of Geophysical Research: Atmospheres*, 102(D14), 16663–16682.
- 738
- 739 Molod, A., Takacs, L., Suarez, M., Bacmeister, J., Song, I.-S., & Eichmann, A.
 740 (2012). The GEOS-5 Atmospheric General Circulation Model: Mean
 741 Climate and Development from MERRA to Fortuna. *Technical Report Series on Global Modeling and Data Assimilation*, 28. Retrieved from
 742 <https://gmao.gsfc.nasa.gov/pubs/docs/Molod484.pdf>
- 743
- 744 Pahlavan, H. A., Wallace, J. M., Fu, Q., & Kiladis, G. N. (2021). Revisiting the
 745 quasi-biennial oscillation as seen in era5. part ii: Evaluation of waves and wave
 746 forcing. *Journal of the Atmospheric Sciences*, 78(3), 693–707.
- 747
- 748 Plumb, R. (1977). The interaction of two internal waves with the mean flow: Im-
 749 plications for the theory of the quasi-biennial oscillation. *Journal of the Atmo-
 750 spheric Sciences*, 34(12), 1847–1858.
- 751
- 752 Randel, W. J., & Wu, F. (1996). Isolation of the ozone qbo in sage ii data by
 753 singular-value decomposition. *Journal of the atmospheric sciences*, 53(17),
 754 2546–2559.
- 755
- 756 Randel, W. J., Wu, F., Russell III, J. M., Roche, A., & Waters, J. W. (1998). Sea-
 757 sonal cycles and qbo variations in stratospheric ch4 and h2o observed in uars
 758 haloe data. *Journal of the atmospheric sciences*, 55(2), 163–185.
- 759
- 760 Rao, J., Garfinkel, C. I., & White, I. P. (2020a). How does the quasi-biennial oscilla-
 761 tion affect the boreal winter tropospheric circulation in cmip5/6 models? *Jour-
 762 nal of Climate*, 33(20), 8975–8996. doi: 10.1175/JCLI-D-20-0024.1
- 763
- 764 Rao, J., Garfinkel, C. I., & White, I. P. (2020b, 05). Impact of the Quasi-Biennial
 765 Oscillation on the Northern Winter Stratospheric Polar Vortex in CMIP5/6
 766 Models. *Journal of Climate*, 33(11), 4787–4813. Retrieved from <https://doi.org/10.1175/JCLI-D-19-0663.1> doi: 10.1175/JCLI-D-19-0663.1
- Rao, J., Garfinkel, C. I., & White, I. P. (2020c). Projected strengthening of the ex-
 767 tratropical surface impacts of the stratospheric quasi-biennial oscillation. *Geo-*

- physical Research Letters, 47(20), e2020GL089149.

Richter, J. H., Anstey, J. A., Butchart, N., Kawatani, Y., Meehl, G. A., Osprey, S., & Simpson, I. R. (2020). Progress in simulating the quasi-biennial oscillation in cmip models. *Journal of Geophysical Research: Atmospheres*, 125(8), e2019JD032362.

Richter, J. H., Solomon, A., & Bacmeister, J. T. (2014). On the simulation of the quasi-biennial oscillation in the community atmosphere model, version 5. *Journal of Geophysical Research: Atmospheres*, 119(6), 3045–3062. doi: 10.1002/2013JD021122

Rind, D., Jonas, J., Balachandran, N. K., Schmidt, G. A., & Lean, J. (2014). The qbo in two giss global climate models: 1. generation of the qbo. *Journal of Geophysical Research: Atmospheres*, 119(14), 8798–8824. Retrieved from <https://agupubs.onlinelibrary.wiley.com/doi/abs/10.1002/2014JD021678> doi: <https://doi.org/10.1002/2014JD021678>

Scaife, A. A., Butchart, N., Warner, C. D., Stainforth, D., Norton, W., & Austin, J. (2000). Realistic quasi-biennial oscillations in a simulation of the global climate. *Geophysical Research Letters*, 27(21), 3481–3484.

Shamir, O., Schwartz, C., Garfinkel, C. I., & Paldor, N. (2021). The power distribution between symmetric and anti-symmetric components of the tropical wavenumber-frequency spectrum. *Journal of the Atmospheric Sciences*, in press. doi: 10.1175/JAS-D-20-0283.1

Shaw, T. A., & Shepherd, T. G. (2007). Angular momentum conservation and gravity wave drag parameterization: Implications for climate models. *Journal of the atmospheric sciences*, 64(1), 190–203.

Shepherd, T. G., & Shaw, T. A. (2004). The angular momentum constraint on climate sensitivity and downward influence in the middle atmosphere. *Journal of the atmospheric sciences*, 61(23), 2899–2908.

Takahashi, M. (1996). Simulation of the stratospheric quasi-biennial oscillation using a general circulation model. *Geophysical Research Letters*, 23(6), 661–664.

Takahashi, M. (1999). Simulation of the quasi-biennial oscillation in a general circulation model. *Geophysical Research Letters*, 26(9), 1307–1310.

Tian, E. W., Su, H., Tian, B., & Jiang, J. H. (2019). Interannual variations of water vapor in the tropical upper troposphere and the lower and middle stratosphere

- 798 and their connections to enso and qbo. *Atmospheric Chemistry and Physics*,
 799 *19*(15), 9913–9926.
- 800 White, I. P., Garfinkel, C. I., Gerber, E. P., Jucker, M., Hitchcock, P., & Rao,
 801 J. (2020). The generic nature of the tropospheric response to sudden
 802 stratospheric warmings. *Journal of Climate*, *33*(13), 5589–5610. doi:
 803 10.1175/JCLI-D-19-0697.1
- 804 Yao, W., & Jablonowski, C. (2013). Spontaneous qbo-like oscillations in an at-
 805 mospheric model dynamical core. *Geophysical Research Letters*, *40*(14), 3772–
 806 3776.
- 807 Yao, W., & Jablonowski, C. (2015). Idealized quasi-biennial oscillations in an en-
 808 semble of dry gcm dynamical cores. *Journal of the Atmospheric Sciences*,
 809 *72*(6), 2201 - 2226. Retrieved from <https://journals.ametsoc.org/view/journals/atsc/72/6/jas-d-14-0236.1.xml> doi: 10.1175/JAS-D-14-0236.1
- 810 Yoo, C., & Son, S.-W. (2016). Modulation of the boreal wintertime madden-julian
 811 oscillation by the stratospheric quasi-biennial oscillation. *Geophysical Research
 812 Letters*, *43*(3), 1392-1398. Retrieved from <https://agupubs.onlinelibrary.wiley.com/doi/abs/10.1002/2016GL067762> doi: <https://doi.org/10.1002/2016GL067762>
- 813 Zhang, C., & Zhang, B. (2018). Qbo-mjo connection. *Journal of Geophysical Re-
 814 search: Atmospheres*, *123*(6), 2957–2967.